JOURNAL OF PHYSICAL ORGANIC CHEMISTRY
J. Phys. Org. Chem. 2001; **14:** 604–611
DOI:10.1002/poc.405

Applications of non-steady-state kinetics in physical organic chemistry: guidelines for the resolution of the kinetics of complex reaction mechanisms

Vernon D. Parker* and Yixing Zhao

Department of Chemistry and Biochemistry, Utah State University, Logan, UT 84322-0300, USA

Received 27 February 2001; revised 20 April 2001; accepted 29 April 2001

ABSTRACT: The resolution of the kinetics of the reversible consecutive second-order reaction mechanism

$$A + B \underset{k_b}{\overset{k_f}{\rightleftharpoons}} I \xrightarrow{k_p} P$$

involving the formation of a kinetically significant intermediate, which does not reach steady state before late in the first half-life, followed by an irreversible product-forming reaction is discussed. It is shown that an apparent second-order rate constant k_{app} and an extent of reaction–time profile are the only experimental data necessary for the evaluation of k_f and k_b (the forward and reverse rate constants) as well as k_p (the microscopic rate constant for the product forming reaction). When the product-forming step involves the cleavage of a C—H bond, for which there is a deuterium kinetic isotope effect on k_p, the resolution of the kinetics is enhanced. In this case, the experimental data include two apparent rate constants ($k_{app}^H$and k_{app}^D) and two extent of reaction–time profiles, one for normal reactants and the other for isotopically substituted reactants. Under these circumstances, a unique highly resolved experimental to theoretical data fit is found that results in the evaluation of all four microscopic rate constants: k_f, k_b, k_p^H and k_p^D. An alternative, when a kinetic isotope effect is not involved, is to fit the extent of reaction–time profiles for two or more concentrations of reactants concurrently. This procedure results in the resolution of the three microscopic rate constants for the reaction. Copyright © 2001 John Wiley & Sons, Ltd.

KEYWORDS: non-steady-state kinetics; complex mechanisms; reaction kinetics

INTRODUCTION

It has recently been shown that some second-order organic reactions that involve the cleavage of C—H bonds take place by two-step mechanisms involving the formation of kinetically significant intermediates.[1,2] The kinetics of the two-step mechanism can be resolved to provide the microscopic rate constant for the formation of the intermediate k_f, as well as those for the partitioning of the intermediate between the reactants (k_b) and the products (k_p). The key to the resolution of the kinetics of the complex mechanisms is that the reactions often do not reach steady state before late in the first half-life. In the *pre-steady-state* time period the various rate constants affect the overall rate of reaction to different extents than implied by the rate equation derived for the steady-state case.

Two examples of reactions for which we have resolved the kinetics are illustrated in Schemes 1 and 2. The first case (Scheme 1) involves the proton transfer reactions between methylarene radical cations and pyridine bases.[1] The other system (Scheme 2) consists of the reaction between a nitroalkane and hydroxide ion to give the stable carbanion.[2] The intermediates are shown in parentheses in Schemes 1 and 2 and are believed to be donor–acceptor complexes. Both studies revealed that the reactions do not reach steady state until late in the first

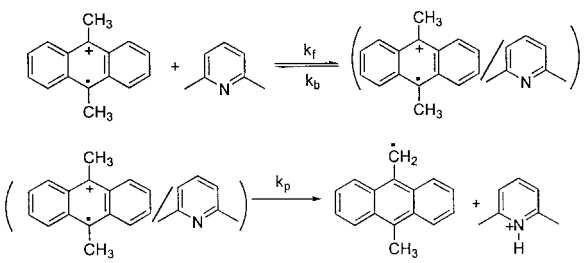

Scheme 1

*Correspondence to: V. D. Parker, Department of Chemistry and Biochemistry, Utah State University, Logan, UT 84322-0300, USA.
E-mail: vparker@cc.usu.edu
Contract/grant sponsor: National Science Foundation; *Contract/grant number:* CHE-0074405.

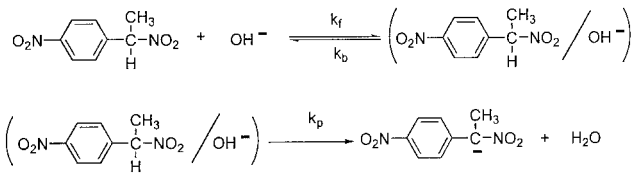

Scheme 2

half-life and were accompanied by extent-of-reaction-dependent apparent deuterium kinetic isotope effects (KIE_{app}). Real deuterium kinetic isotope effects (KIE_{real}) derived from the resolved rate constants for proton and deuteron transfer were observed to be considerably larger than KIE_{app} in both cases. The latter suggests that the extent of proton tunneling is considerably greater in these reactions than could have been concluded from the KIE_{app}.

In this paper we systematically develop the use of non-steady-state kinetics as a powerful tool in physical organic chemistry to identify complex reaction mechanisms and to resolve the apparent rate constants into the microscopic rate constants for the elementary steps in the mechanism.

RESULTS AND DISCUSSION

Reversible second-order consecutive mechanisms

In mechanism (1)

$$\mathrm{HA} \underset{k_b}{\overset{k_f'}{\rightleftharpoons}} \mathrm{I} \xrightarrow{k_p} \mathrm{C} \qquad (1)$$

the general analytical solution of the set of three differential equations for the rate expressions for the three species, in terms of the initial reactant concentration $[HA]_0$ and the rate constants, consists of the set of Eqns (2a)–(2c)

$$[\mathrm{HA}] = [\mathrm{HA}]_0(\lambda_2 - \lambda_1)^{-1}\{(k_b + k_p - \lambda_1) \times \exp(-\lambda_1 t) - (k_b + k_p - \lambda_2)\exp(-\lambda_2 t)\} \qquad (2a)$$

$$[\mathrm{I}] = [\mathrm{HA}]_0 k_f (\lambda_2 - \lambda_1)^{-1} \times \{\exp(-\lambda_1 t) - \exp(-\lambda_2 t)\} \qquad (2b)$$

$$[\mathrm{C}] = [\mathrm{HA}]_0\{1 + k_f k_p(\lambda_1 - \lambda_2)^{-1}\exp(-\lambda_1 t) + k_f k_p[\lambda_2(\lambda_2 - \lambda_1)]^{-1}\exp(-\lambda_2 t)\} \qquad (2c)$$

for the instantaneous concentrations [HA], [I] and [C] respectively,[3,4] where $\lambda_1\lambda_2 = k_f' k_p$ and $(\lambda_1 + \lambda_2) = k_f' + k_b + k_p$. Note that in reaction 1 k_f', a first-order or pseudo first-order rate constant, is labeled to distinguish it from the second-order rate constants in the other equations. When the formation of the product C is monitored the pertinent equation is Eqn. (2c). Equation (2c) can be used to calculate extent of reaction–time profiles for the pseudo first-order version of mechanism (3a). The differential equations for the irreversible second-order sequence (3b) have been solved using a separation of variables technique, which may possibly be applicable to reaction (3a).[5]

$$\mathrm{HA} + \mathrm{B} \underset{k_b}{\overset{k_f}{\rightleftharpoons}} \mathrm{I} \xrightarrow{k_p} \mathrm{C} \qquad (3a)$$

$$\mathrm{HA} + \mathrm{B} \xrightarrow{k_f} \mathrm{I} \xrightarrow{k_p} \mathrm{C} \qquad (3b)$$

$$\mathrm{HA} + \mathrm{B} \xrightarrow{k_f} \mathrm{C} \qquad (3c)$$

The differential equations describing consecutive bimolecular reactions, e.g. mechanisms (3a) and (3b), are classified as non-linear, and general analytical solutions cannot be found.[4] The analytical solution is available for the irreversible second-order reaction (3c).[6–9] On the other hand, a general Laplace transform methodology for solving kinetic schemes of unimolecular transformations has been reported.[4] Integrated rate equations for a number of mechanisms can be found in several monographs.[6–9]

The lack of an analytical solution for the kinetics of reaction (3a) makes it necessary to resort to numerical integration in order to obtain extent of reaction–time profiles under second-order conditions. When applying numerical methods there is no need to treat reactions (3a) and (3b) as distinct mechanisms. Mechanism (3b) is a limiting case of mechanism (3a) when k_b becomes insignificantly small relative to k_p. In the remainder of this discussion the latter is assumed.

Methodology

The fourth-order Runge–Kutta method[10] is commonly used for numerical integration of complex rate equations and was selected for the derivation of the extent of reaction–time profiles discussed here. No significant differences between the data obtained using the analytical Eqn. (2c) and that obtained by numerical integration could be detected under conditions where both methods are applicable. A pertinent description of the use of the fourth-order Runge–Kutta integration in chemical kinetics, with an example, can be found in a monograph dealing with the determination of organic reaction mechanisms.[9] A more general brief introduction to the application of numerical integration methods in chemical kinetics can be found in a recent text-book.[11]

Care must be taken to determine whether or not the set of differential equations that is being solved numerically is "stiff".[12] (Research on numerical methods that addressed

the problem of stiff systems of equations in chemical kinetics peaked in the 1970s, and an entire issue of the *Journal of Physical Chemistry* was devoted to this topic in 1977.[12]) Stiff systems of equations result for mechanism (3a) when the rate of one of the three reactions is several orders of magnitude different than the other two.

In practice we use two different methods to insure that our numerical integrations are reliable. The first is to compare results obtained using the fourth-order Runge–Kutta method with simple finite difference (Euler's method) integrations. The numerical integration results for stiff systems of equations will differ using the two methods, with the finite difference method giving the greatest error. For systems of equations that are not stiff, the two methods result in values that do not differ significantly as long as the time step is sufficiently small. When we suspect possible stiff behavior we compare our results with those obtained using commercially available programs that have the capability to handle stiff systems of equations.[†] The complex proton transfer reactions that we have encountered so far do not give rise to stiff behavior, and the usual numerical methods are applicable to the integrations.

In order to generate the extent of reaction–time profiles we typically carry out calculations with reaction times changing incrementally between calculations so that about 50 000 calculations are necessary to reach an extent of reaction equal to 0.50. For example, if the half-life of the reaction is 5 s then the first calculation is at $t = 0.0001$ s. The reaction time is then incremented by 0.0001 s ($t = 0.0002$ s) for the second calculation and calculations are repeated until the extent of reaction for the last calculation is >0.50. The times for extents of reaction equal to 0.05, 0.06, 0.07, 0.08, 0.09, 0.10, 0.15, 0.20, 0.25, 0.30, 0.35, 0.40, 0.45 and 0.50 are then determined from the data and a data file consisting of 14 extent of reaction/time points is constructed. The 14 data points for analysis correspond to those we use in experimental studies. The data file is then used to compare with an appropriate experimental file during the procedure to find the best fit between experimental and theoretical data.

We usually avoid taking data points at times earlier than necessary for the extent of reaction to equal 0.05. There can be a considerable degree of uncertainty in data recorded at short times when using stopped-flow spectrophotometry to follow the course of the reaction. This uncertainty arises from the time necessary for mixing of reactant solutions. For example, if the "dead-time" is 3 ms then the error in time is large at 10 ms, but it is considerably less significant at 100 ms.

[†] During the 1990s programs capable of providing accurate integration results for stiff systems of equations became commercially available. The two that we use to compare our results with are DIGISIM (electrochemical applications) and BERKELEY MADONNA (stopped-flow homogeneous kinetics). The programs are based on semi-implicit algorithms with variable time-step size. Neither program is directly applicable to our data-fitting procedure, but they serve the purpose of insuring that our calculations are reliable.

In the sections that follow we demonstrate the method used to fit theoretical extent of reaction–time profiles to the corresponding experimental data. Theoretical extent of reaction–time profiles using systematic variations in the trial values of the rate constants are simulated and the sum of the deviations between theoretical and experimental data is determined for each calculated profile. The best fit is then determined to be the calculated profile that shows the lowest value of the total deviation between the calculated and experimental data.

Comparison of the extent of reaction–time profiles for the reversible consecutive mechanism with that for the irreversible second-order mechanism

Once steady state is reached the rate law for mechanism (3a) is given by Eqn. 4. If we compare this with the rate law in Eqn. 5 for the irreversible second-order mechanism (3c) we see that the two rate laws are experimentally indistinguishable and only differ in the definitions of the rate constants.

$$d[C]/dt = [k_f k_p/(k_p + k_b)][HA][B] \quad (4)$$

$$d[C]/dt = k_f[HA][B] \quad (5)$$

On the other hand, in the period before steady state is established the rate constants for mechanism (3a) affect the overall rate of the reaction to degrees different than implied by Eqn. 4. The latter gives rise to extent of reaction–time profiles in the pre-steady-state period that can differ significantly from that for the irreversible second-order mechanism.

We begin by examining the extent of reaction-time profiles for reaction (3a) when $[HA]_0 = 0.0001$ M and $[B]_0 = 0.002$ M, with $k^H_{app} = 99.8\ M^{-1}s^{-1}$, $k^D_{app} = 13.9\ M^{-1}\ s^{-1}$, $k_f = 139\ M^{-1}\ s^{-1}$ and with several different values of k^H_p.The rate constants used, with the exception of the

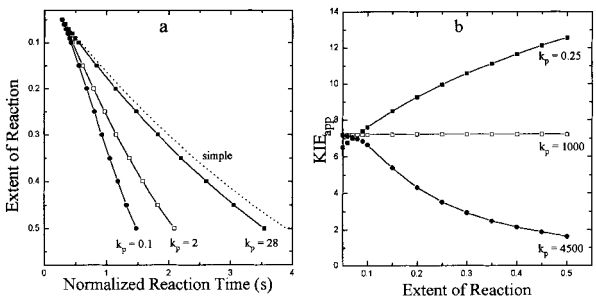

Figure 1. Extent of reaction–time profiles (a) and apparent kinetic isotope effect–extent of reaction profiles (b) for the two-step proton transfer mechanism as a function of proton transfer rate constant. [HA] = 0.001 M, [B] = 0.002 M, $k^H_{app} = 99.8\ M^{-1}\ s^{-1}$, $k^D_{app} = 13.9\ M^{-1}\ s^{-1}$

variable k_p, are those that were derived for the reaction between 1-nitro-1-(4-nitrophenyl)ethane ($NNPE_{H(D)}$) and hydroxide ions in water/acetonitrile (50/50 vol.%) at the reactant concentrations given.[2] The parameters were chosen to insure that the theoretical data generated are pertinent to a known reaction. The extent of reaction–time profiles in Fig. 1a are for the HA/B reaction. The dashed line in Fig. 1a represents the response for the simple second-order mechanism. The essential message that can be derived from these data is that extent of reaction–time profiles for mechanism (3) are generally more steep than those for the irreversible second-order mechanism (3c). A comparison of an experimental extent of reaction–time profile with that expected for the irreversible second-order reaction provides a convenient criterion for mechanism analysis.

The second experimental test to distinguish between complex and simple mechanism behavior for a reaction involving the cleavage of a C—H(D) bond consists of plotting KIE_{app} (equal $(k^H_{app})_{ss}/(k^D_{app})_{ss}$, where the subscript ss indicates a steady-state value) versus the extent of reaction. This analysis is illustrated in Fig. 1b, for the same set of parameters as before, with three widely different k_p values. The data show that, in the pre-steady-state period, KIE_{app} for mechanism (3a) can increase, remain constant, or decrease with increasing extent of reaction. Again, these plots provide an additional convenient criterion for mechanism analysis.

Fitting experimental to theoretical extent of reaction–time profiles

Experimental non-steady-state kinetic studies of reactions involving C—H bond cleavage provide extent of reaction–time profiles as well as apparent rate constants for the HA (k^H_{app}) and DA (k^D_{app}) reactions. For a single extent of reaction–time profile (either HA or DA data), the relationship between the apparent rate constant and the microscopic rate constants is given by Eqns 6 or 7.

$$(k^H_{app})_{ss}/k_f = (k^H_p/k_b)/(1 + k^H_p/k_b) = C_H \qquad (6)$$

$$(k^D_{app})_{ss}/k_f = (k^D_p/k_b)/(1 + k^D_p/k_b) = C_D \qquad (7)$$

When both HA and DA profiles are available the KIE_{real} can be derived from Eqn. 8.

$$KIE_{real} = [C_H/(1 - C_H)]/[C_D/(1 - C_D)] = k^H_p/k^D_p \quad (8)$$

The definitions in terms of C_H and C_D are used to emphasize that the determination of KIE_{real} requires only values of k_f and the apparent rate constants.

We have previously shown[1] that the range of k_f where resolution of the non-steady-state kinetic data can be accomplished is approximately from k_{app} to 11 times k_{app}.

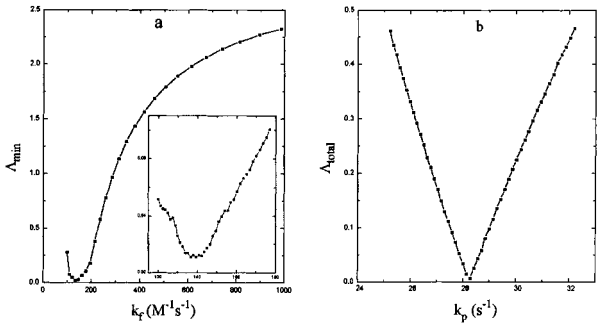

Figure 2. Fitting curves for the HA extent of reaction–time profile where k_f (a) or k_p (b) is varied to find the best fit. [HA] = 0.0001 M and [B] = 0.002 M. The comparison file consisted of the extent of reaction–time profile generated with $k^H_{app} = 99.8\ M^{-1}\ s^{-1}$, $k_f = 139\ M^{-1}\ s^{-1}$ and $k_p = 28.2\ s^{-1}$. Λ is defined in Eqn. 9. The inset plot has higher resolution on the k_f axis

The protocol for the fitting of experimental to theoretical data is the same whether a single extent of reaction–time profile is available, or extent of reaction–time profiles for both HA and DA reactions are available. A number of k_f values over the entire applicable range are selected and, at each k_f, k^H_p is varied while adjusting the other rate constant(s) (k_b or k_b and k^D_p) to conform to Eqns (6)–(8). The latter results in an array of extent of reaction–time profiles, one for each k^H_p value at each k_f value. For example, we typically do calculations for 25 k_f with 50 k^H_p at each k_f for the first iteration of the fitting procedure, resulting in 1250 extent of reaction–time profiles. Since 50000 calculations are involved in each extent of reaction–time profile, an enormous number of calculations are carried out just in the first iteration. However, the calculations do not require excessive computer time: the 25 $k_f \times 50\ k_p$ extent of reaction–time profile array only requires about 25 s using a 850 MHz Pentium III processor.

In the discussion of Figs 2–7 that follows, the "experimental" data file is made up of theoretical data

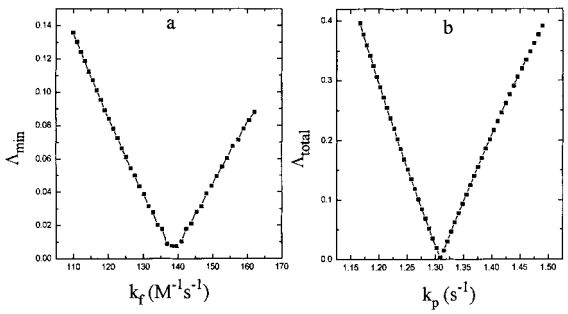

Figure 3. Fitting curves for the DA extent of reaction–time profile where k_f (a) or k_p (b) is varied to find the best fit. [DA] = 0.0001 M and [B] = 0.002 M. The comparison file consisted of the extent of reaction–time profile generated with $k^D_{app} = 13.9\ M^{-1}\ s^{-1}$, $k_f = 139\ M^{-1}\ s^{-1}$ and $k_p = 1.31\ s^{-1}$. Λ is defined in Eqn. 9

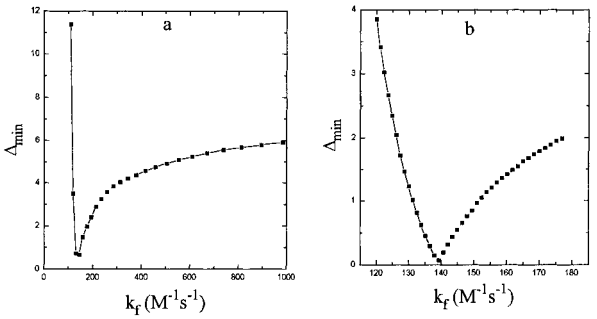

Figure 4. Concurrent fitting curves for the HA and DA extent of reaction–time profiles from Figs 2 and 3. The comparison file consisted of the two extent of reaction–time profiles with $k_{app}^{H} = 99.8\ M^{-1}\ s^{-1}$, $k_{app}^{D} = 13.9\ M^{-1}\ s^{-1}$, $k_f = 139\ M^{-1}\ s^{-1}$, $k_p^{H} = 28.2\ s^{-1}$, and $k_p^{D} = 1.31\ s^{-1}$. Curves (a) and (b) differ in the resolution on the k_f axis. Δ is defined in Eqn. (10)

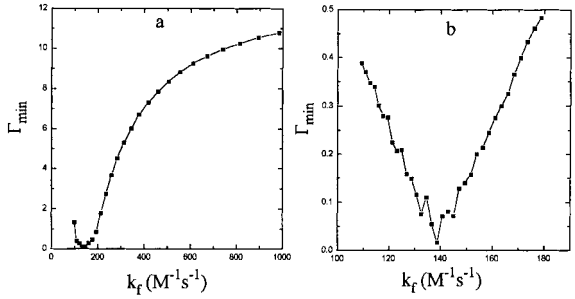

Figure 6. Fitting curves for the HA extent of reaction–time profiles for [B] equal to 0.005 and 0.0005 M. [HA] was equal to 0.0001 M. The comparison file consisted of the extent of reaction–time profile generated with $k_{app}^{H} = 99.8\ M^{-1}\ s^{-1}$, $k_f = 139\ M^{-1}\ s^{-1}$ and $k_p = 28.2\ s^{-1}$. Curves (a) and (b) differ in the resolution on the k_f axis. Γ is defined in Eqn. (11)

calculated for [HA] = [HD] = 0.0001 M, [B] = 0.002, 0.005 or 0.0005 M, $k_{app}^{H} = 99.8\ M^{-1}\ s^{-1}$, $k_{app}^{D} = 13.9\ M^{-1}\ s^{-1}$, $k_f = 139\ M^{-1}\ s^{-1}$, $k_p^{H} = 28.2\ s^{-1}$, and $k_p^{D} = 13.9\ s^{-1}$. These data were generated to correspond to those reported in table 1 of Ref. 2 for the reaction of $NNPE_{H(D)}$ with hydroxide ions in water/acetonitrile (50/50 vol.%) at 298 K. The input data are summarized in Table 1. Using this data file as input illustrates the fitting process without distraction from experimental error in the kinetic data.

The first step for determining the best fit of the calculated data to the input data, usually experimental data, but in this case that summarized in Table 1, involves the determination of the deviation between the calculated extent of reaction–time points and those in the input file. The output for comparison is the total deviations Λ_{total}, defined in Eqn. 9, between the two data arrays (input and calculated).

$$\Lambda_{total} = 100 \sum_{1}^{14} [(t_{calc}^{ER} - t_{file}^{ER})/t_{file}^{ER}]/14 \qquad (9)$$

The terms t_{calc}^{ER} and t_{file}^{ER} are the times to reach a given extent of reaction (ER) in the calculated profile and in the input profile respectively. The summation is over extents of reaction corresponding to 0.05, 0.06, 0.07, 0.08, 0.09, 0.10, 0.15, 0.20, 0.25, 0.30, 0.35, 0.40, 0.45 and 0.50. A Λ_{total} is recorded for each calculated extent of reaction–time profile.

Suppose that the data array consists of extent of reaction–time profiles for 50 k_p values at each k_f value. The procedure to find the best fit is to first plot Λ_{total} versus k_p for each k_f. For a given k_f the minimum of the resulting Λ_{total}/k_p plot gives the best-fit value of k_p and the corresponding Λ_{min} (Λ_{total} at the minimum) for that k_f. The procedure provides an array of 25 data points (one for each k_f), and plotting Λ_{min} versus k_f results in a V-shaped curve that gives the best-fit value of k_f at the minimum. The data-fitting procedure is demonstrated in the following sections.

Fitting single extent of reaction–time profiles to theoretical data for the complex mechanism

The fitting procedure was carried out on the extent of

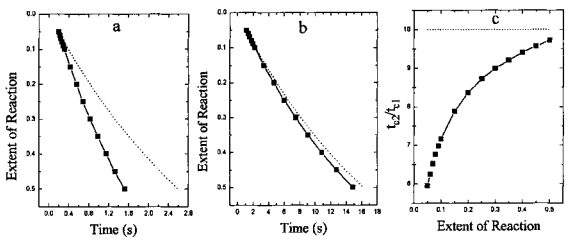

Figure 5. Extent of reaction–time profiles for HA with B at [B] equal to 0.005 M (a) and 0.0005 M (b). Data generated with $k_{app}^{H} = 99.8\ M^{-1}\ s^{-1}$, $k_f = 139\ M^{-1}\ s^{-1}$ and $k_p = 28.2\ s^{-1}$. The time ratios t_D/t_H in curve (c) are times for a specific extent of reaction for curve (b) divided by the corresponding time for curve (a)

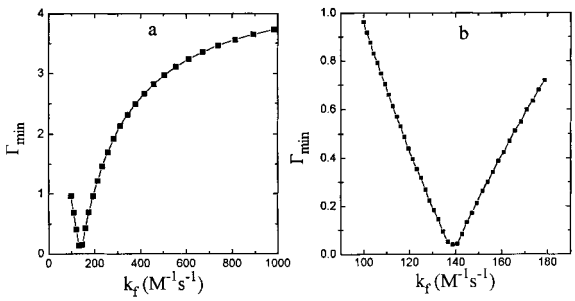

Figure 7. Fitting curves for the DA extent of reaction–time profiles for [B] equal to 0.005 and 0.0005 M. [DA] was equal to 0.0001 M. The comparison file consisted of the extent of reaction–time profile generated with $k_{app}^{D} = 13.9\ M^{-1}\ s^{-1}$, $k_f = 139\ M^{-1}\ s^{-1}$ and $k_p = 1.31\ s^{-1}$. Curves (a) and (b) differ in the resolution on the k_f axis

Table 1. Input file parameters for experimental to theoretical data fitting used in Figs 1–7

Parameter	Value	Application
$k_f/M^{-1}\ s^{-1}$	139	Figs 1–7
$k_{app}^{H}/M^{-1}s^{-1}$	99.8	Figs 1, 2, 4, 5, 6
$k_{app}^{D}/M^{-1}s^{-1}$	13.9	Figs 1, 3, 4, 5, 7
k_p^{H}/s^{-1}	28.2	Figs 1, 2, 4, 5, 6
k_p^{D}/s^{-1}	1.31	Figs 1, 3, 4, 5, 7
[HA] = [DA]/M	0.0001	Figs 1–7
[B]/M	0.0020	Figs 1–4
[B]/M	0.005, 0.0005	Figs 5–7

reaction–time profiles for the HA reactions with B and the results are summarized in Fig. 2. The curve in Fig. 2a was derived from extent of reaction–time profiles generated from 25 k_f, over the range from k_{app}^{H} to 10 k_{app}^{H}, with 50 k_p values at each k_f. For each k_f a Λ_{min} was derived from the corresponding k_p versus Λ_{total} plots. The k_f at the minimum of the plot is the best fit value at the resolution of the plot. The inset provides a higher degree of resolution on the k_f axis and a second-order polynomial fit of the data in the region of the minimum results in $(k_f)_{min} = 139\ M^{-1}\ s^{-1}$. In order to obtain the best fit value of k_p, a new set of 50 extent of reaction–time profiles was generated with $k_f = 139\ M^{-1}\ s^{-1}$ and k_p ranging from about 25 to 32 s^{-1}. The resulting plot of Λ_{total} versus k_p is shown in Fig. 2b. The minimum in this plot is very close to 28.2 s^{-1} on the k_p axis, which is the expected best-fit value.

Similar calculations were carried out on the DA reaction with the input data summarized in Table 1. The array of 1250 extent of reaction–time profiles was generated as in the previous paragraph. The plot of Λ_{min} versus k_f shown in Fig. 3a gives k_f at the minimum of a V-shaped curve very close to $139\ M^{-1}\ s^{-1}$ without further refinement of the calculations. The Λ_{total} versus k_p plot shown in Fig. 3b is again very close to the expected best-fit value of 1.31 s^{-1}.

Concurrent fitting of extent of reaction–time profiles for HA and DA to theoretical data for the complex mechanism

When there are two extent of reaction–time profiles in the input file the total deviation between experimental and theoretical data files can be expressed as in Eqn. (10)

$$\Delta_{total} = \Delta_{total}^{HA} + \Delta_{total}^{DA} + \Delta_{total}^{KIE} \qquad (10)$$

where each of the three terms on the right-hand side are defined in a manner similar to the definition of Λ_{total} in Eqn. 9. The first iteration of the fit of the HA + DA input file to theoretical data is illustrated in Fig. 4a for extent of reaction–time profiles where k_f was varied from k_{app}^{H} to 10 k_{app}^{H}. In order to determine the best-fit k_f value it was desirable to increase the resolution of the k_f axis, and the results are illustrated by the plot in Fig. 4b, where k_f is varied from about 120 to $180\ M^{-1}\ s^{-1}$. The minimum of this curve falls very close to the expected value of $139\ M^{-1}\ s^{-1}$.

It is of interest to note the relatively large values of Δ_{min} that give rise to the deep minima when the HA and DA data are treated concurrently. The best-fit values of the rate constants can readily be obtained under these circumstances, even when there is significant experimental error in the extent of reaction–time profiles.

Extent of reaction–time profiles for reactions of HA with B at two concentrations

In previous work we have only considered the resolution of proton transfer kinetics where extent of reaction–time profiles could be obtained for reactions of both HA and DA.[1,2] If the resolution of the kinetics requires data from reactions of both HA and DA this would be a serious limitation, in that only reactions showing significant deuterium kinetic isotope effects could be treated by the non-steady-state kinetic method. We find that the latter is not the case, since concurrent analysis of either HA or DA reactions at two or more different concentrations makes use of two or more extent of reaction–time profiles for the analysis. The extent of reaction–time profiles for the reactions of HA (0.0001 M) with B at two different concentrations are shown in Fig. 5a ([B] = 0.005 M) and b ([B] = 0.0005 M). The dashed lines in Fig. 5a and b represent the extent of reaction–time profile for the irreversible second-order mechanism. When the ratios of times t_{C2}/t_{C1} (subscripts C2 and C1 refer to the two concentrations) for each of the data points are plotted versus extent of reaction the curve illustrated in Fig. 5c is generated. The expected result for a second-order reaction at steady state is that $t_{C2}/t_{C1} = 10.0$ and independent of the extent of reaction. The fact that the curve in Fig. 5c deviates significantly from this behavior is a consequence of the fact that in the pre-steady-state time period the rate constants affect the overall rate of the reaction to a different extent than implied by the rate law of Eqn. 4. Obviously, this suggests that the deviations from simple mechanism behavior of reaction profiles obtained at two different reactant concentrations (C1 and C2) in the pre-steady-state time period, together with the corresponding t_{C2}/t_{C1}–extent of reaction plot (Fig. 5c), give rise to mechanistic information similar to that illustrated in Fig. 1 for isotopically different reactants.

Concurrent fitting of extent of reaction–time profiles for two different reactant concentrations

The input file in this case consists of the extent of reaction–time profiles for the two different base concentrations. The fitting procedure is exactly the same when the input data are extent of reaction–time profiles for isotopically substituted reactants. The total deviation between experimental (input file) and theoretical data can be expressed as:

$$\Gamma_{\text{total}} = \Gamma^{\text{C2}}_{\text{total}} + \Gamma^{\text{C1}}_{\text{total}} + \Gamma^{\text{C2/C1}}_{\text{total}} \qquad (11)$$

The terms on the right-hand side of Eqn. (11) have the same significance as the comparable terms in Eqn. (10).

The plot in Fig. 6a represents the first iteration of the fit of the input file for the reaction of HA with B, at [B] equal 0.005 (C1) and 0.0005 M (C2), over a range of k_f from $k^{\text{H}}_{\text{app}}$ to ten $k^{\text{H}}_{\text{app}}$. The plot of Γ_{total} versus k_f has a minimum very near the expected value, 139 $\text{M}^{-1}\,\text{s}^{-1}$. The plot from a new set of calculations with increased resolution on the k_f axis is shown in Fig. 6b. At this resolution there is some scatter in the plot, but the minimum is clearly very close to the expected value. The reason for the scatter is likely connected with the fact that Γ_{total} is made up three different terms and the relative values of these may vary slightly with changes in k_f.

The input file for the reaction of DA with [B] at the same concentrations used for the reactions of HA is fit with data calculated over the same range of k_f, from $k^{\text{H}}_{\text{app}}$ to 10 $k^{\text{H}}_{\text{app}}$, in Fig. 7a. Even at the k_f resolution used, it would be possible to make an accurate estimate of k_f from this plot. The plot shown in Fig. 7b is for a second set of calculations at higher resolution on the k_f axis. The minimum of this plot is very near the expected value on the k_f axis, 139 $\text{M}^{-1}\,\text{s}^{-1}$.

The illustration of the data-fitting procedure in Fig. 7 clearly shows that the analysis of the same reaction at two different reactant concentrations is equivalent to the analysis of extent of reaction–time profiles for two isotopically substituted reactants in terms of the variation from simple mechanism behavior in the time period before steady state is achieved.

Three different symbols for the total deviations between experimental and theoretical extent of reaction–time data are used in Eqns (9)–(11), despite the fact that they have similar definitions. This is to emphasize that the terms on the right-hand sides of the equations differ.

The effect of reversibility and isotopic exchange on the extent of reaction–time profiles for the simple second-order reaction

Reversibility of a simple second-order proton transfer reaction and isotopic exchange can also give rise to deviations of extent of reaction–time profiles from that expected for the irreversible second-order mechanism. It is important that we establish the degree and direction of deviations due to the latter in order to see whether or not these deviations could be confused with complex mechanism behavior. Isotopic exchange has previously led to erroneous conclusions during proton transfer studies. The very large deuterium kinetic isotope effects reported by Caldin and coworkers[13–15] for the reaction of 4-nitrophenylnitromethane with tetramethylguanidine ($(Me_2N)_2C{=}NH$), a strong organic base with an exchangeable N—H, inspired further study. Reinvestigations of the reaction revealed that the results reported for the D-labeled acid are unreliable owing to proton/deuteron (H/D) exchange and that the apparent deuterium kinetic isotope effect was lowered to about 11 when the base was changed to $(Me_2N)_2C{=}ND$.[16,17] The latter conclusion was later[18] confirmed using tritium kinetic isotope effects.

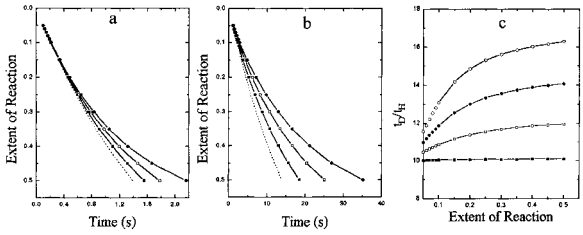

Figure 8. The effect of the reverse reaction (a) and H/D exchange (b) on extent of reaction–time profiles for HA (a) and DA (b) for reactions of 0.0001 M acid with 0.005 M base. The dashed line is for the simple irreversible second-order reaction. The solid lines are for the two-step mechanism of HA (a) and DA (b) with $k^{\text{H}}_{\text{f}} = 100\ \text{M}^{-1}\,\text{s}^{-1}$, $k^{\text{D}}_{\text{f}} = 10\ \text{M}^{-1}\,\text{s}^{-1}$. The reverse reaction rate constant k_b was equal to 28.2 (filled squares), 14.1 (open squares) and 7.05 s^{-1} (filled circles)

The extent of reaction–time profiles for HA (0.0001 M) and B (0.005 M), assuming the simple reversible second-order mechanism with $k^{\text{H}}_{\text{f}} = 100\ \text{M}^{-1}\text{s}^{-1}$ and k_b equal to 28.2, 14.1 and 7.05 s^{-1}, are illustrated in Fig. 8a. The dashed line is the extent of reaction–time profile for the irreversible second-order mechanism. All of the lines for the reversible mechanism lie above that for the irreversible reaction. The extent of reaction–time profiles for the reaction of DA with B under the same conditions with k^{D}_{f} equal to $10\ \text{M}^{-1}\,\text{s}^{-1}$ are shown in Fig. 8b. The value of k_b was assumed to be the same for both HA and DA reactions. The latter implies that there is total isotopic exchange for the DA reaction. All three of the extent of reaction–time profiles for the reversible reaction in Fig. 8a and Fig. 8b lie above the dashed line representing the simple irreversible extent of reaction–time profile.

The ratio of the times to reach specific values of the extent of reaction for the DA reaction to that for the HA reaction, t_D/t_H, are plotted versus the extent of reaction in

Fig. 8c. These curves are similar to those shown in Fig. 1b and could be mistaken to be indicative of complex mechanism behavior. However, since the extent of reaction–time profiles for the reversible/exchange case (Fig. 8a and b) deviate in the opposite sense from the deviation due to complex mechanism behavior (Fig. 1a), the two different mechanisms cannot be confused using the non-steady-state kinetics method.

CONCLUSIONS

The kinetics of reactions involving the cleavage of a C—H bond are frequently second-order, dependent upon the concentrations of the substrate and another reagent, and appear to conform to an irreversible single-step mechanism. These reactions often pass through kinetically significant intermediates that go undetected using conventional kinetic analyses. There is increasing evidence[1,2] that many of these reactions do not reach the steady state before late in the first half-life. When this is the case the kinetics of the reactions can be resolved into the microscopic rate constants for the elementary steps by carrying out analysis in the *pre-steady-state* time period. In this paper we have outlined how deviations between experimental extent of reaction–time profiles and those expected for the irreversible second-order mechanism can be used to show that the kinetics do not conform to the latter mechanism. The experimental extent of reaction–time profiles can be fit to theoretical data for the reversible consecutive mechanism to show conformity to the latter. When the reaction is accompanied by a deuterium kinetic isotope effect, the concurrent analysis of extent of reaction–time profiles provides increased resolution in the data-fitting process. Alternatively, extent of reaction–time profiles obtained at two or more reactant concentrations can provide increased resolution.

Acknowledgements

This research was supported by the National Science Foundation (CHE-0074405). We gratefully acknowledge this support.

REFERENCES

1. Parker VD, Zhao Y, Lu Y, Zheng G. *J. Am. Chem. Soc.* 1998; **120**: 12 720–12 727.
2. Zhao Y, Lu Y, Parker VD. *J. Am. Chem. Soc.* 2001; **123**: 1579–1586.
3. Johnston HS. *Gas Phase Reaction Rate Theory*. The Ronald Press: New York, NY, 1966; 329.
4. Andraos J. *J. Chem. Ed.* 1999; **76**: 1578–1583.
5. Anderson RL, Nohr RS, Spreer LO. *J. Chem. Ed.* 1975; **52**: 437–438.
6. Capellos C, Bielski BHJ. *Kinetic Systems: Mathematical Description of Chemical Kinetics in Solution*. Wiley: New York, 1972.
7. Rodiguin NM, Rodiguina EN. *Consecutive Chemical Reactions: Mathematical Analysis and Developments*. Van Nostrand: Toronto, 1981.
8. Moore JW, Pearson RG. *Kinetics and Mechanism*. Wiley: New York, 1981.
9. Carpenter BK. *Determination of Organic Reaction Mechanisms*. Wiley: New York, 1984.
10. Milne WE. *Numerical Solution of Differential Equations*. Wiley, New York, 1953; 72–73.
11. Steinfeld JI, Francisco JS, Hase WL. *Chemical Kinetics and Dynamics*. Prentice Hall: New Jersey, 1999; chapter 2.
12. Young TR, Boris JP. *J. Phys. Chem.* 1977; **81**: 2424–2427.
13. Caldin EF, Mateo S. *Chem. Commun.* 1973; 854–855.
14. Caldin EF, Mateo S. *J. Chem. Soc. Faraday Trans.* 1975; **71**: 1876–1904.
15. Caldin EF, Mateo S, Warrick P. *J. Am. Chem. Soc.* 1981; **103**: 202–204.
16. Rogne O. *Acta Chem. Scand.* 1978; 559–563.
17. Kresge AJ, Powell MF. *J. Phys. Org. Chem.* 1990; **3**: 55–61.
18. Kresge AJ, Powell MF. *J. Am. Chem. Soc.* 1981; **103**: 201–202.